Materials Science Forum
ISSN: 1662-9752, Vol. 1091, pp 3-13
doi:10.4028/p-5ncgbk

Submitted: 2022-08-11
Revised: 2022-12-04
Accepted: 2022-12-04
Online: 2023-06-05

A Novel Non-Invasive Cryostatic Spectrometry Technique to Characterize the Carriers' Multiplication Factor in Silicon Carbide Power Devices

Marco Pocaterra[a], Mauro Ciappa[b*]

ETH Zurich, Integrated Systems Laboratory, Zurich, Switzerland

[a]pocmarco@iis.ee.ethz.ch, [b]ciappa@iis.ee.ethz.ch

Keywords: Terrestrial cosmic radiation, Failure rate, Power SiC devices reliability, Carriers' multiplication, Spectrometry under cryostatic conditions

Abstract. The design of robust power semiconductor devices and the assessment of their susceptibility to terrestrial cosmic rays induced failures requires the accurate characterization of the device-internal electric field. This work presents a non-invasive cryostatic spectrometry technique making use of a soft-gamma Am^{241} radioactive source, to sense the device-internal electric field of silicon carbide power devices, through the measurement of the carriers' multiplication factor. *TCAD* and *Monte Carlo* simulations tools are coupled to predict the soft-gamma irradiation spectra and to localize the hotspots for charge multiplication in the device structure. An empirical relationship is derived to convert the carriers' multiplication factor measured at cryogenic temperature to the multiplication factor at ambient temperature. Finally, by highlighting the correlation between the multiplication factor and the failure rate of power devices exposed to terrestrial cosmic radiation, the technique is proposed as a complimentary method for the on-field assessment of the *Safe-Operating Area*.

1- Introduction

Silicon Carbide (*SiC*) power devices have been observed to be susceptible to insidious failure mechanisms as single-event burnouts (*SEB*) when exposed by terrestrial cosmic radiation (*TCR*) [1]–[5]. This is the case for both *SiC Schottky Diodes* and *MOSFETs* rated over 1 kV*,* that have been observed to fail at similar rates when exposed to cosmic neutrons in the same biasing conditions, suggesting a fundamentally similar failure mechanism in both the device types [6].

The strength of the device-internal electric field, that is the driver of the carriers' multiplication, is a major factor in determining the failure rate of devices exposed to *TCR* [7], [8]. To ensure the robustness of *SiC* power devices against *TCR* induced failures, the electric field at the blocking junctions needs to be accurately characterized.

Recently, the irradiation of power devices with radioactive sources has been proposed as a technique to characterize the internal electric field of *SiC* components through the measurement of carriers' multiplication [9]–[11]. Special focus has been devoted to a non-invasive technique that makes use of Am^{241} as a soft-gamma radiation source [12], [13]. By exposing devices biased in the blocking state to the soft-gamma source, the technique has proven to be effective provided that the reverse current in the device under test (*DUT*) is much lower than the peak of the ionization current generated by a single absorbed photon. At ambient temperature (*AT*), this condition is fulfilled in such devices and in biasing conditions where the thermal generation of carriers is particularly low. However, in a variety of *SiC* devices the thermal noise dominates the useful signal, restricting the applicability of the technique to a limited number of *DUTs*.

In this work, this limitation has been removed by carrying out measurements at liquid nitrogen temperature (*LNT*, 77 K) and converting the obtained carriers' multiplication factor to the operating temperature of the device. A novel spectroscopy setup has been developed, that makes use of a dedicated high-voltage capable cryostat, operating at 77 K. An empirical relationship is derived to convert the multiplication factor measured at *LNT* to the multiplication factor at the operating

temperature. The experimental technique is demonstrated on the set of *SiC* commercial devices listed in Table 1.
Additionally, an original simulation scheme, based on the coupling of *TCAD* and *Monte Carlo* tools, is used to accurately predict the measured irradiation spectra and to localize the multiplication hotspots within the device structure.
In Section 2 and 3, the experimental setup and the original simulation scheme are presented, respectively. Section 4 discusses the experimental and simulation results, deriving the empirical relationship to convert the *LNT* multiplication factor to *AT*. Here, the correlation of the carriers' multiplication factor and the *TCR* induced failure rate assessed in literature [14] by neutron irradiation is discussed.

2- The experimental Setup.

The working principle. The working principle of the proposed technique can be summarized as follows. A *SiC* device (*JBS* diode or *MOSFET*) is biased in the blocking state while kept at *LNT* and irradiated with a collimated beam of soft-gamma particles from an Am^{241} radioactive source to generate electron-hole pairs in the depletion region of the main blocking junction. The charge carriers are separated by the local electric field and eventually multiplied by impact ionization, generating a current pulse at the device terminals, that is collected by a dedicated spectrometer. Every single pulse is then processed offline to extract the related pulse charge and to build a pulse charge spectrum.
For every *DUT*, spectra are collected for different biasing conditions, starting from a voltage for which no charge multiplication occurs, and the device is in full-depletion conditions (typically around 30% of the breakdown voltage of the *DUT*), up to close breakdown conditions (90% of the breakdown voltage). The carriers' multiplication factor is assessed based on the shift of the spectra referred to the spectrum acquired in no multiplication conditions, according to [9].

The measurement setup. A block representation of the measurement setup employed in this work is given in Fig. 1(a). The different components are discussed in the following section.

The high-voltage cryostat. At the front-end of the measurement setup, the *DUT* is biased in the blocking state using a high-voltage power supply operated at ambient temperature and insulated from the net by a power-line transformer. The *DUT* is enclosed in a dedicated cryostat, whose structure is shown in Fig. 1(b), alongside with the Am^{241} compact source. The cryostat consists of a 25 liters Dewar, partially filled with liquid nitrogen, in which an aluminum bracket acts as an efficient heat conductor between the liquid and the *DUT*. The bias voltage is carried to the *DUT* by a shielded coaxial cable traversing a 1 cm large hole machined in the polystyrene lid of the Dewar. The aluminum bracket and the Dewar's metallic enclosure are grounded to ensure safety and to generate an efficient Faraday cage that shields to *DUT* from *EM* noise. The *DUT* temperature, acquired over 800 hours of operation, is stable within 1 K.

Table 1. Specifications of the investigated samples and related tests

Sample	Tech.	Rating (*AT*)	V_{BD} (*AT*)	V_{BD}(*LNT*)	Tests
JBS_1	4H-SiC	1.7 kV, 35 A	2.26 kV	2.070 kV	*AT, LNT*
MOS_1	4H-SiC Gen 2	1.7 kV, 72 A	2.35 kV	2.263 kV	*AT, LNT*
MOS_2	4H-SiC Gen 2	1.2 kV, 36 A	1.70 kV	1.630 kV	*AT, LNT*
MOS_3	4H-SiC Gen 3	1.2 kV, 32 A	1.61 kV	1.520 kV	*LNT*
MOS_4	4H-SiC Gen 3	1.0 kV, 32 A	1.27 kV	1.130 kV	*LNT*

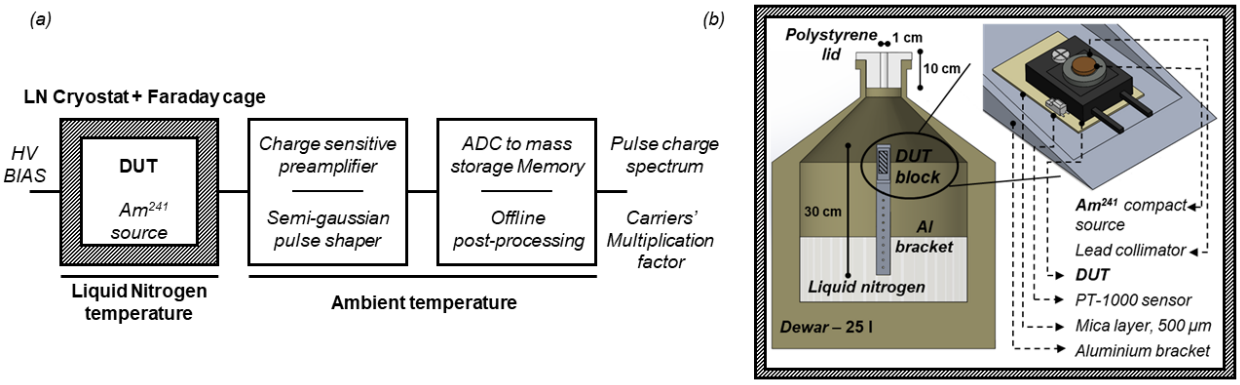

Fig. 1 (a) Block representation of the cryostatic spectrometer. (b) Sketch of the high-voltage cryostat with the compact Am^{241} radioactive source.

The Am^{241} radioactive source. The experimental setup employs a collimated (exempt-quantity) compact Am^{241} radioactive source, with an activity lower than 37 kBq. Am^{241} exhibits an almost monoenergetic gamma emission at 59.5 keV. In the present application, the soft-gamma transition is used to form the collimated ionizing beam that induces the generation of charge pairs at the *DUT* blocking junction. Fig. 2 shows the gamma emission spectrum of the Am^{241} source, as measured by a 250 µm thick silicon photodiode, alongside the attenuation of gamma radiation in *SiC*. The 59.5 keV photons from the Am^{241} source interact with *SiC* by photoelectric effect and by incoherent scattering with comparable probability. In the present case, the relevant interaction mechanism is the photoelectric effect, which results in the almost uniform generation of 59.5 keV secondary photoelectrons across the full depth of the irradiated *DUT*. Incoherent scattering results in the generation of secondary electrons whose energy is at least six times smaller than the one of the photoelectrons [12] and can be neglected as the amount of equivalent deposited charge is below the detection limit of the spectrometer. Fig. 3(a) reports the *Monte Carlo* simulation of the interaction of 59.5 keV photoelectrons with *SiC*, showing that their range does not exceed 18 µm and that 90% of their kinetic energy is released almost isotopically within 12 µm from the interaction point of the soft-gamma particle. This allows for a quite local generation of electron-hole pairs, localized in the depleted region of the *DUTs*. The use of the Am^{241} soft-gamma source for the measurement of charge multiplication has been preferred to other irradiation techniques as it allows for many different advantages.

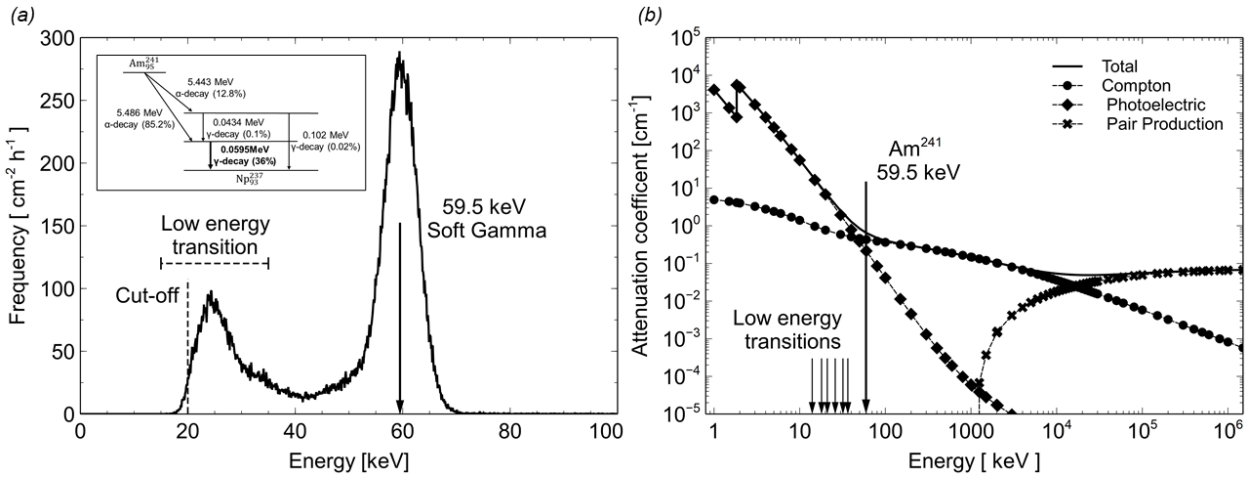

Fig. 2 (a) Photopeak at 59.5 keV of the Am^{241} source, as measured by a Silicon photodiode at ambient temperature. Insert: simplified Am^{241} decay scheme. (b) Attenuation of gamma radiation in SiC by the different interaction mechanisms. The most relevant interaction for the 59.5 keV soft-gamma transition of Am^{241} is the Photoelectric effect, since the Compton scattering produces secondary electrons with negligible energy.

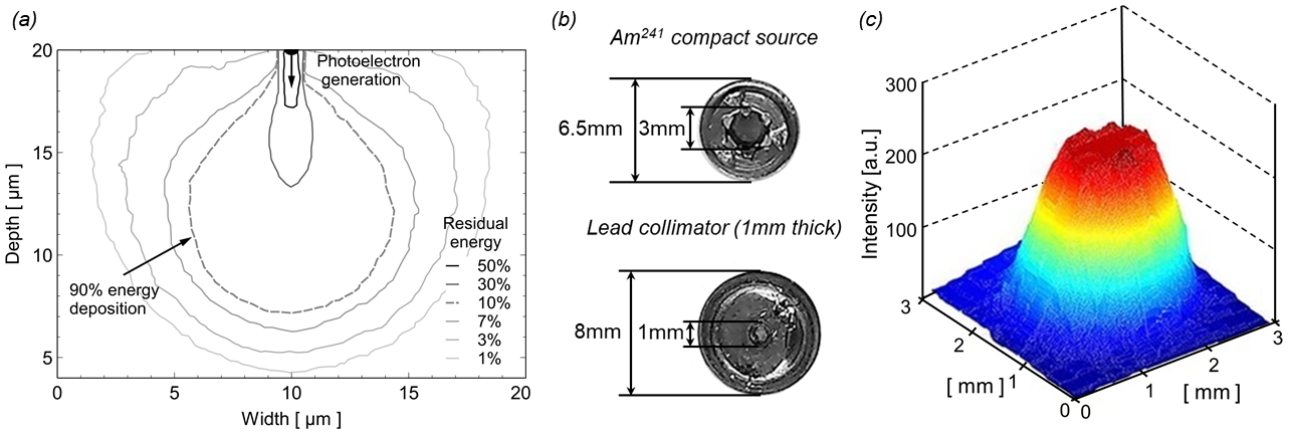

Fig. 3 (a) Monte Carlo simulation of the energy deposition area by 59.5 keV photoelectrons in SiC, as percentage of the residual electron energy. (b) The Am^{241} compact source and the lead collimator. (c) Photoradiography of the beam spot at the chip surface through the 2 mm epoxy package, after collimation.

Compared to alpha irradiation techniques, using the soft-gamma approach allows to operate with packaged *DUTs*, whose pristine state is not altered by decapsulation procedures. Furthermore, alpha particles exhibit a limited range that in some cases cannot produce carriers generation over the full width of the depletion layer [15]. This is not the case for the secondary photoelectrons generated by Am^{241} soft-gamma radiation, whose low charge deposition does not alter the steady-state device-internal electric field. Compared to emitters that provide gamma particles of higher energy (e.g., Co^{60}, Cs^{137}), Am^{241} allows to limit the interaction volume of the particles to around 18 µm, preventing unwanted long-range effects. Furthermore, it ensures ease of collimation by a compact lead collimator. Co^{60} and Cs^{137}would require lead collimators whose thickness is in the order of centimeters. This is not the case for the soft-gamma emission of Am^{241}. Fig. 3(b) shows the lead collimator employed in this application. As shown in Fig. 3(c), the 1 mm thick lead collimator allows to attenuate 99% of the intensity of the gamma radiation and to achieve a 1.8 mm beam spot at the surface of the *DUT*, when the source is placed on top of the package of the *DUT*. This allows to irradiate selectively the active area of the device, avoiding spurious signal originating from the irradiation of the termination region. The Am^{241} source has also been preferred to an *x-ray* generator, as its compactness is essential to fit in the high-voltage cryostat and its emission does not exhibit an unwanted *bremsstrahlung* component.
The advantages exhibited by the soft-gamma emission of Am^{241}come at the price that the charge generated by every single ionization interaction is small (about 1.2 fC in *SiC*) and so the use of the cryostat is essential to achieve good *SNR* in the charge pulse acquisitions.

The spectrometry chain. The *DUT* is connected to a dedicated spectrometry chain, that is operated at ambient temperature. The spectrometer employed in the experimental setup is described in very detail in [16]. Its functioning can be summarized as follows. The *DUT*'s high-voltage terminal is *AC*-coupled to the first stage of the spectrometry chain. This is a charge sensitive preamplifier that converts the current pulses collected at the *DUT* terminals to voltage signals, employing a high-bandwidth (250 MHz) trans-impedance amplifier followed by a high-bandwidth voltage amplifier. The preamplifier is followed by a shaping amplifier with an 8 µs shaping time, consisting in a *Sallen-Key* second-order active band-pass filter with pole-zero cancellation, that adapts the bandwidth of the pulse signal to the sampling rate of the following *ADC*, while providing noise and pile-up rejection. The output signal of the shaping amplifier is acquired by a *14*-bit *ADC* and stored in a solid-state memory for offline post-processing. Details of the post-processing procedures are given in [16].
The main source of noise affecting the measurement setup originates from the fluctuations of the leakage current in the *DUT* [16], so from the thermal generation of carriers in its depletion region. Employing the high-voltage cryostat reduces by at least two orders of magnitude the thermal current of the tested *DUTs*, compared to the ambient temperature case, strongly reducing the intensity of the

leakage current fluctuations, and improving the accuracy of the spectrometer. Under these conditions, the resolution of the spectrometer is mainly limited by the capacitance of the *DUT* and allows to acquire charge pulses down to 0.5 fC with a 4% resolution.

3- TCAD and Monte Carlo Simulations.

A dedicated simulation scheme that couples *TCAD* and *Monte Carlo* tools has been developed for the simulation of single-event soft-gamma interaction with the *SiC* devices investigated in this work. Here, the discussion is limited to the case of a *SiC JBS* diode, as the results for a *SiC MOSFET* of the same voltage class do not differ significantly.

A simulation model, given in Fig. 4(a), has been implemented in the *TCAD* simulation environment of Sentaurus Device [17]. This model is representative for the *SiC JBS* diode (JBS_1) investigated experimentally. Fig. 4(b) and (c) present the principles of the simulation procedure. At first, the dependency of the multiplication factor on the position within the *DUT* of the charge deposition and on the applied reverse voltage has been calculated by the sequential *TCAD* simulation of the transport of a probe charge deposited in the vertices of a regular grid defined across the active region. The simulation occurs as follows. The single *JBS* cell model is brought to a reverse bias condition via quasi-static voltage steps. Once reached a selected bias condition, a probe charge is injected in the position of interest and the transport of the excess charge is simulated by a transient analysis. Charge multiplication is assessed by integrating the current pulse originating at the device terminals following the charge injection, normalized to the initial charge injected. The probe charge is calibrated to allow for minimal distortion of the steady-state electric field, while ensuring reasonable simulation times. The probe charge injection is achieved by a dedicated *C++* code implemented in the *Sentaurus Physical Model Interface* [17]. The following simulation step consists in a *Monte Carlo* process that accounts for the charge generated along the ionization track of a photoelectron in the *SiC JBS* cell, as shown schematically in Fig. 4(c). The simulation starts with a random process generating the interaction site of every single gamma photon according to a uniform distribution, reasonable due to the low attenuation of photons in the target material. A second random process defines the angle of the emission direction of the secondary photoelectron, starting from the interaction location of the primary photon. The emission direction is assumed uniform (-180°, 180°). The third phase of the *Monte Carlo* process deals with the density of carriers generated by the photoelectron along its ionization track. For the sake of simplicity, the generated carriers' density is assumed as uniform along the whole length of the ionization track, while the initial energy is generated based on the experimental spectra of the gamma emission of Am^{241} (Fig. 2(a)). The length of the ionization track is assumed to be 18 µm, based on the *Monte Carlo* simulation of the interaction of photoelectrons

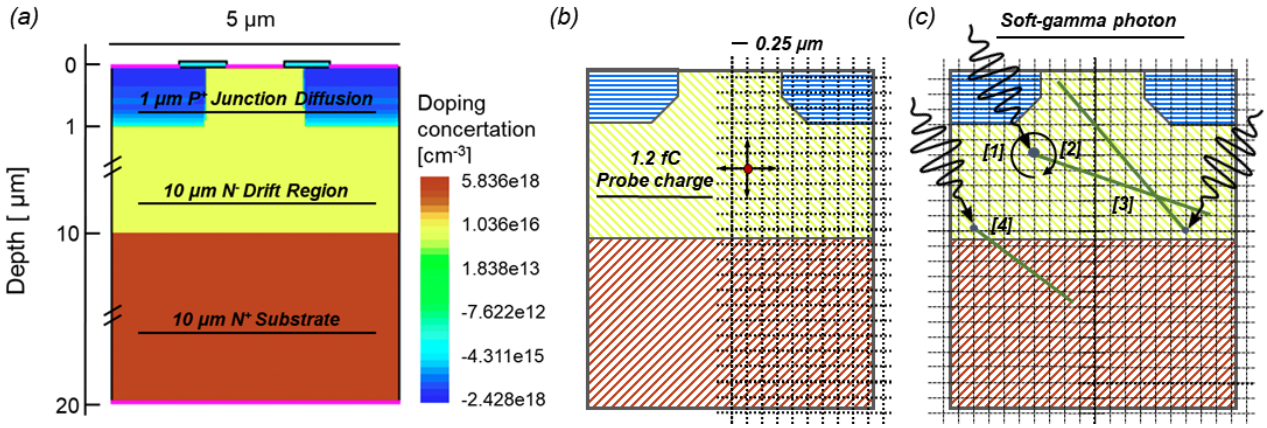

Fig. 4 (a) TCAD simulation model of a single cell SiC JBS diode. (b-c) Coupled TCAD-Monte Carlo simulation scheme. (b) Grid for TCAD simulation using probe charges of the dependency on the site of the multiplication (c) Random process for the determination of the interaction site of a soft-gamma photon and of the emission angle of the related photoelectron. 1-Interaction site, 2-Emission angle (-180°-180°), 3- Length of the ionization track:18 µm, 4- Ionization track leading to incomplete charge collection.

with *SiC*, shown in Fig. 3(a). The multiplication factor referred to a given interaction event is obtained by integrating along the ionization track produced by every single photoelectron the interpolated 3D-function calculated by the *TCAD* simulation in the first phase of the procedure.
A spectrum, for a given biasing condition, is finally obtained by iterating this procedure to calculate the distribution of the charge generated by several thousand of soft-gamma interaction events.

4- Results.

The experimental spectra. Fig. 5 reports the experimental spectra resulting from the irradiation with Am^{241} soft-gamma particles at *LNT* of some selected devices of Table 1. As the reverse bias applied to the blocking junction increases, the spectra shift towards higher charges due to carriers' multiplication. To avoid the saturation of the spectrometer due to an excessive count-rate, a *cut-off* is applied to low-intensity pulses that results in the low-side truncation of the experimental spectra acquired at increased voltage bias. The *SiC DUTs* exhibit a spectrum that is significantly different from the ones acquired in the same irradiation conditions in the case of silicon-based devices of comparable rating. This is mainly due to the difference in the thickness of the depletion region. While the range of 59.5 keV photoelectrons in silicon and *SiC* is comparable, the thickness of the depletion region of *SiC* devices is eight to ten times smaller compared to the silicon counterparts of comparable rating. In the case of silicon devices rated 1.2 kV or more, the energy released by the secondary photoelectrons is frequently completely absorbed in the depletion region. This is not the case for the *SiC* devices investigated here, as the thickness of their fully depleted depletion region (10-15 μm) is comparable to the range of the secondary photoelectrons and only a part of their energy is effectively collected. This fundamental difference is further empathized by the simulation results in the following section.

The TCAD-Monte Carlo simulation. Fig. 6(a) reports the soft-gamma spectra resulting from the simulation scheme described previously, applied to the *SiC JBS* diode model of Fig. 4(a). Fig. 6(b) reports the results of the same kind of simulation carried out for a *Si PiN* diode model of the same voltage rating, for comparison purposes.
As shown in the experimental spectra of the previous section, at high blocking voltage values, the spectra show tails in the high charge section generated by interaction events resulting in large multiplication values. In the case of the silicon device, due to the thickness of the depletion region, the multiplication factor only slowly depends on the interaction site of the soft-gamma photon. In its spectrum this results in a photopeak which maintain its shape while shifting towards higher charges as the reverse bias increases.

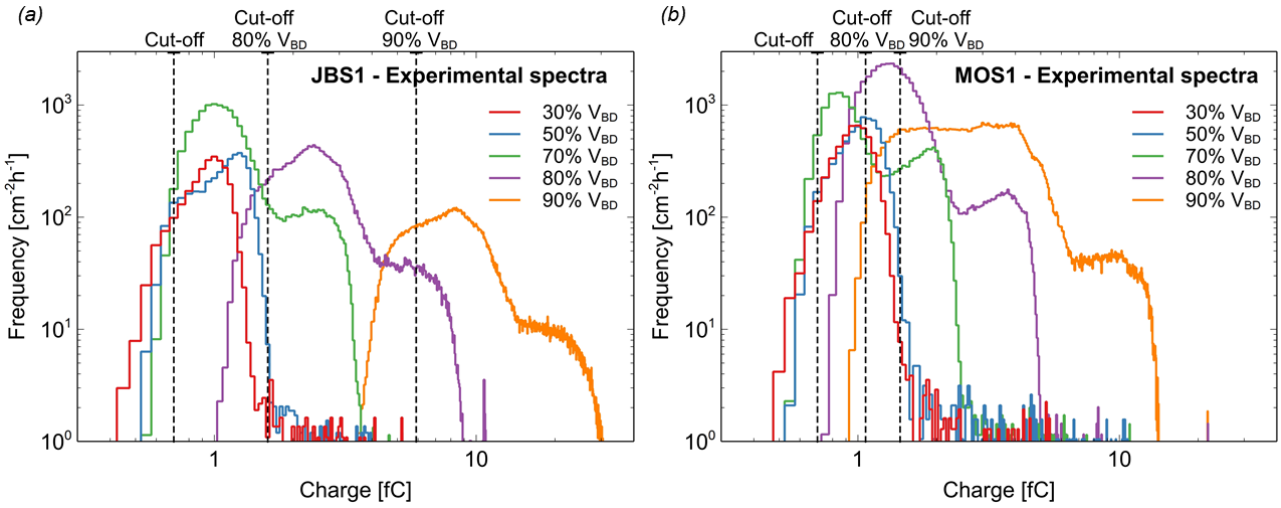

Fig. 5 Experimental pulse chare spectra resulting from the irradiation with the Am^{241} soft-gamma source at LNT of (a) JBS_1 and (b) MOS_1, at different normalized reverse biases V_{BIAS}/V_{BD}.

The simulation scheme allows to locate the origin of such events. Fig. 6(c) shows a map of the simulated multiplication factor as a function of the soft-gamma interaction site and photoelectron emission angle, for the *SiC JBS* model.
In the case of the *SiC JBS* diode, the incomplete collection of the charge generated by the soft-gamma interaction results in a greater statistical spread and pulses of lower intensity. Furthermore, a multiplication is observed that depends more strongly than in the silicon case on the interaction site of the gamma photon, as highlighted in the map of Fig. 6(c). Therefore, the formation of a complete photopeak is not observed in the *SiC* device case. Intense peaks of multiplication are observed in the case of soft-gamma interactions in the close vicinity of the N^-N^+ junction. This effect is in consequence of the fact that in *SiC* the impact ionization coefficient of holes is larger than for electrons, and holes generated at this location can be accelerated across the whole thickness of the depleted region, undergoing massive multiplication. This observation is dual in the case of the silicon-based device, for which peaks of multiplication are observed in proximity of the P^+N^- junction.

The multiplication factor at operating temperature. Some *DUTs* (e.g., *JBS1*, *MOS1* and *MOS2*) already exhibit a sufficiently low level of thermal generated reverse current at ambient temperature that allows for the measurement of the charge multiplication by soft-gamma irradiation. This fact allows for a comparison of the multiplication factor measured at *LNT* to the one measured at *AT*, shown in Fig. 7(a) for *JBS1*, *MOS1* and *MOS2*. Here, the applied reverse bias voltage has been normalized with respect to the breakdown voltage of the *DUT*, measured at the respective temperature.

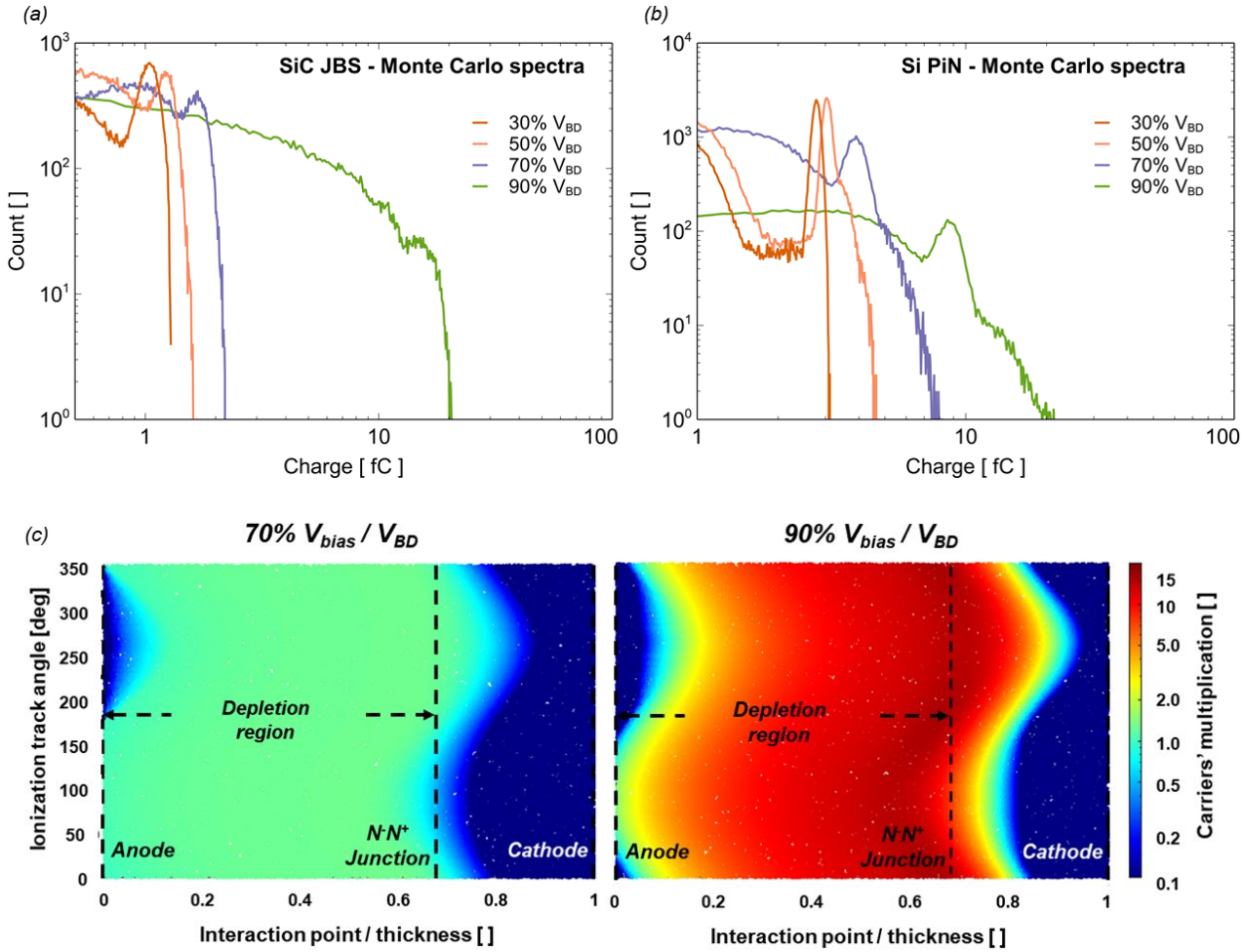

Fig. 6 Pulse charge spectra simulated by the coupled TCAD-Monte Carlo scheme of (a) SiC JBS diode, (b) Si PiN diode. (c) Carriers' multiplication map along the symmetry axis of the model as a function of the normalized emission depth and angle of the photoelectron, for 70% and 90% V_{BIAS}/V_{BD}.

By such normalization, it is observed that the multiplication curves are almost superimposed, within the limit of experimental accuracy. This suggests that the charge multiplication factor is essentially a function of the normalized bias V_{BIAS} / V_{BD}. This observation is corroborated by *Miller's empirical formula*, expressing the multiplication factor (M) in step junctions [18]:

$$M(V) = \frac{1}{1-\left(\frac{V}{V_{BD}}\right)^n}. \quad (1)$$

Where V is the reverse bias voltage and n is a fitting exponent. Furthermore, V_{BD} is an expression for the breakdown voltage, which includes implicitly its dependency on the temperature.
The dependency of the carriers' multiplication factor on the normalized bias V_{BIAS} / V_{BD} has also been investigated by *TCAD* simulation. For this scope, the transport and multiplication of carriers in the *SiC JBS* of Fig. 4(a) has been simulated according to the procedure described in the Section 3 for different temperature values (300-580 K), within the validity range of the *Hatakeyama* [19] (hydrodynamic) model for the avalanche generation of carriers by impact ionization.
The simulations show that, in the investigated temperature range, the multiplication of carriers decreases with increasing temperature following the reduction of the mean free path for carriers. Nevertheless, as shown in Fig. 7(b), the multiplication factor shows almost no dependence on temperature once represented as a function of the normalized bias voltage V_{BIAS} / V_{BD}, with peak variations in the 3.5% range.
Following the previous considerations, an empirical relationship is derived for the conversion of the multiplication factor measured at *LNT* to the multiplication factor at operating temperature:

$$M_{HT}(V_{HT}) = M_{LT}(V_{LT}) = M_{LT}\left(V_{HT} \times \frac{V_{BD-LT}}{V_{BD-HT}}\right). \quad (2)$$

Where $V_{BD\text{-}LT}$ and $V_{BD\text{-}HT}$ are the breakdown voltages of the device at *LNT* and operating temperature, respectively.

Correlation of the multiplication factor to the failure rate of devices exposed to TCR. In [14], *Lichtenwalner et al.* carried out accelerated tests of *SiC* power devices by neutron irradiation, revealing that the *TCR* induced *SEB* failure rate of *SiC MOSFETs* and diodes exhibits a universal

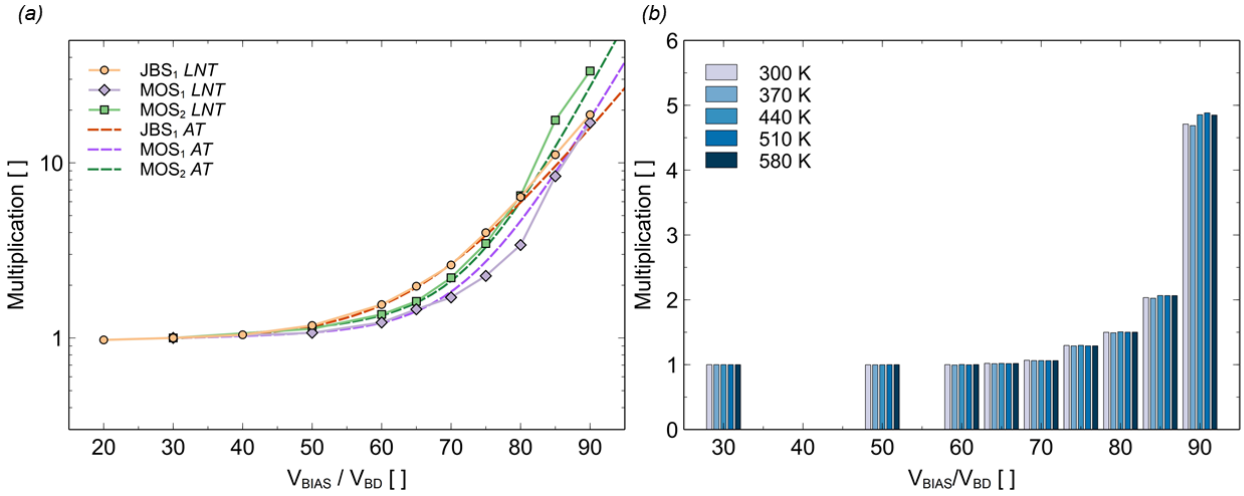

Fig. 7 (a) Experimental charge multiplication factors measured at LNT and AT for JBS1, MOS1 and MOS2, as a function of the normalized reverse bias V_{BIAS}/V_{BD}. By this normalization the curves at ambient temperature almost overlap the curves at measured at cryostatic conditions. (b) TCAD simulation of dependency on the temperature of the multiplication of a probe charge injected at 5 μm depth along the symmetry axis of the SiC JBS diode in Fig. 4(a). Under normalization of the reverse bias V_{BIAS}/V_{BD}, the multiplication just slightly depends on the temperature over the whole validity range of the Hatakeyama Model [19] *for impact ionization.*

scaling behavior as a function of the normalized reverse bias voltage V_{BIAS} / V_{BD}. Recent works [12], [13], have demonstrated the correlation between the *TCR* failure rate of power devices assessed by neutron irradiation and the multiplication factor measured by soft-gamma irradiation at ambient temperature. Although the latter technique has proven to be very promising, its application at room temperature was limited to those devices with a low level of reverse current. Fig. 8(a) shows the multiplication factor as measured by soft-gamma irradiation at *LNT* for all the *DUTs* listed in Table 1. Here, the multiplication factor is given also for *DUTs (*e.g., *MOS3)* that exhibit excessive levels of reverse current at ambient temperature for the accurate measurement of multiplication, demonstrating the improved versatility of the technique granted by the cryostatic operation of the spectrometer. For all the investigated samples, the multiplication factor scales with the normalized bias V_{BIAS} / V_{BD}.
Fig. 8(b) reports about the correlation of the multiplication factor as measured by soft-gamma irradiation at *LNT* to the failure rate assessed according to the universal scaling function introduced by *Lichtenwalner et al.* in [14]. The failure rate is shown to increase as the multiplication factor increases, in a similar fashion for all the investigated samples. Furthermore, the failure rate rapidly increases in the multiplication range from 1 to 1.5-2, where the value of about 100 FIT/cm^2 is reached. Starting from this multiplication level, the failure rate (λ) seems to slow down, converging to a similar trend line, expressed by:

$$\lambda(M) = A\,(M)^B. \tag{3}$$

Where A= 177.5 FIT/cm^2 and B = 0.917.
The observed scaling behavior suggests the possibility of describing the failure rate as a function of the multiplication factor according to a universal law, similarly to what has been proposed in the literature for the normalized bias V_{BIAS}/V_{BD} [14]. In this case, the characterization of the multiplication factor by the Am^{241} soft-gamma source could become a complementary technique to the traditional assessment methods based on neutrons or heavy ions irradiations [5], [14], [20], [21], as well as an efficient tool for the definition of the *Safe operating area* of semiconductor power devices.

5- Summary and Conclusions.

The soft-gamma emission of an Am^{241} radioactive source has been used in conjunction with a dedicated cryostatic spectrometry setup to sense the device-internal electric field of *SiC* power devices, by the measurement of the carriers' multiplication factor. Thanks to the novel setup, measurements of the multiplication factor have been extended to devices that could not be characterized at ambient temperature.

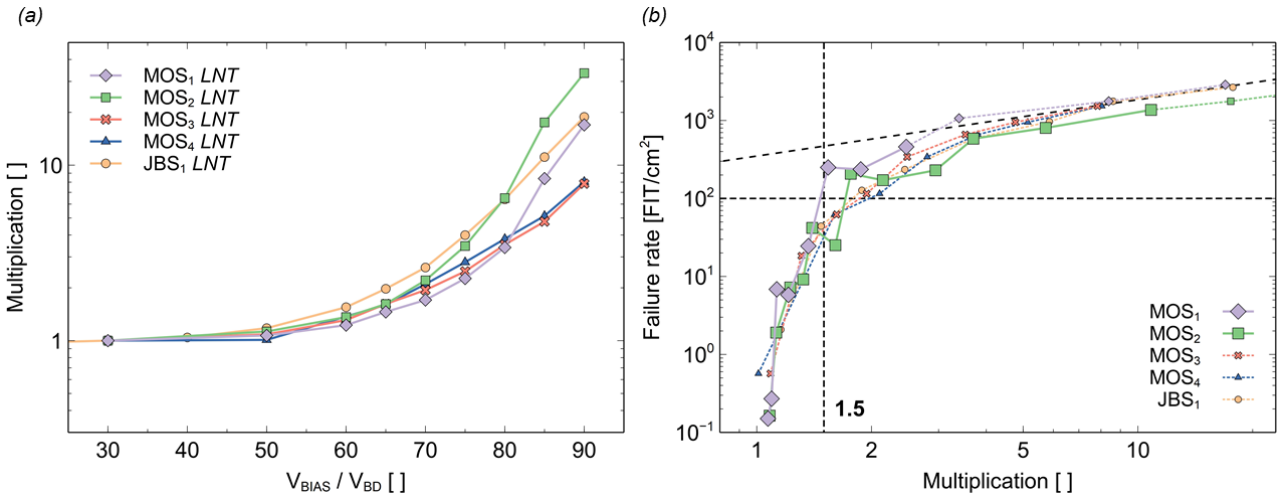

Fig. 8 (a) Multiplication as function of V_{BIAS}/V_{BD} of the devices in Table 1, as measured at liquid nitrogen temperature. (b) Correlation of the measured multiplication to the TCR failure rate, from [14]. *Continuous line: measured failure rate. Dashed line: failure rate estimated from the universal scaling function for SiC power devices* [14].

An empirical relationship has been proposed to convert the multiplication factor measured at cryogenic temperatures to the one at operating temperature. A dedicated simulation scheme, which couples *TCAD* and *Monte Carlo* simulations has been developed and used to simulate efficiently the observed spectra and to locate the multiplication hotspots occurring in power devices.
Finally, the multiplication factor of a set of sample *DUTs* as measured by soft-gamma irradiation has been correlated to the *TCR* induced *SEB* failure rate as measured by neutron irradiation, showing the possibility of describing the failure rate as a function of the multiplication factor according to a universal law, opening some new perspective for the use of the proposed technique for the definition of the *Safe Operating Area* of power devices operated under the influence of terrestrial cosmic rays.

References

[1] G. Soelkner, “Ensuring the reliability of power electronic devices with regard to terrestrial cosmic radiation,” *Microelectron. Reliab.*, vol. 58, pp. 39–50, Mar. 2016, doi: 10.1016/j.microrel.2015.12.019.

[2] D. R. Ball *et al.*, “Effects of Breakdown Voltage on Single-Event Burnout Tolerance of High-Voltage SiC Power MOSFETs,” *IEEE Trans. Nucl. Sci.*, vol. 68, no. 7, pp. 1430–1435, Jul. 2021, doi: 10.1109/TNS.2021.3079846.

[3] A. Akturk *et al.*, “Predicting Cosmic Ray-Induced Failures in Silicon Carbide Power Devices,” *IEEE Trans. Nucl. Sci.*, vol. 66, no. 7, pp. 1828–1832, 2019, doi: 10.1109/TNS.2019.2919334.

[4] H. Kono, T. Ohashi, T. Noda, and K. Sano, “Impact of Device Structure on Neutron-Induced Single-Event Effect in SiC MOSFETs,” *Mater. Sci. Forum*, vol. 963, pp. 738–741, Jul. 2019, doi: 10.4028/www.scientific.net/MSF.963.738.

[5] C. Martinella *et al.*, “Impact of Terrestrial Neutrons on the Reliability of SiC VD-MOSFET Technologies,” *IEEE Trans. Nucl. Sci.*, vol. 68, no. 5, pp. 634–641, May 2021, doi: 10.1109/TNS.2021.3065122.

[6] A. Akturk, R. Wilkins, and J. McGarrity, “Terrestrial neutron induced failures in commercial SiC power MOSFETs at 27C and 150C,” in *IEEE Radiation Effects Data Workshop*, 2015, vol. 2015-Novem, pp. 1–5, doi: 10.1109/REDW.2015.7336737.

[7] T. Oda, T. Arai, T. Furukawa, M. Shiraishi, and Y. Sasajima, “Electric-Field-Dependence Mechanism for Cosmic Ray Failure in Power Semiconductor Devices,” *IEEE Trans. Electron Devices*, vol. 68, no. 7, pp. 3505–3512, 2021, doi: 10.1109/TED.2021.3077208.

[8] D. J. Lichtenwalner, D. A. Gajewski, S. H. Ryu, B. Hull, S. Allen, and J. W. Palmour, “Gate Bias Effects on SiC MOSFET Terrestrial-Neutron Single-Event Burnout,” *Mater. Sci. Forum*, vol. 1062, pp. 463–467, May 2022, doi: 10.4028/p-4b1mb3.

[9] M. Ciappa and M. Pocaterra, “Characterization of the onset of carrier multiplication in power devices by a collimated radioactive alpha source,” *Microelectron. Reliab.*, vol. 100–101, Sep. 2019, doi: 10.1016/j.microrel.2019.06.035.

[10] M. Ciappa and M. Pocaterra, “Measurement of the Pre-Breakdown Characteristics in Silicon Carbide Power Devices by the Use of Radioactive Gamma Sources,” 2020, doi: 10.1109/IRPS45951.2020.9128885.

[11] M. Ciappa and M. Pocaterra, “On the use of Po210and Am241collimated alpha sources for the characterization of the onset of carrier multiplication in power devices,” *Proc. Int. Symp. Phys. Fail. Anal. Integr. Circuits, IPFA*, vol. 2020-July, 2020, doi: 10.1109/IPFA49335.2020.9260952.

[12] M. Ciappa and M. Pocaterra, "On the use of soft gamma radiation to characterize the pre-breakdown carrier multiplication in SiC power MOSFETs and its correlation to the TCR failure rate as measured by neutron irradiation," *Microelectron. Reliab.*, vol. 114, no. October, p. 113838, 2020, doi: 10.1016/j.microrel.2020.113838.

[13] M. Ciappa and M. Pocaterra, "Assessing the pre-breakdown carriers' multiplication in SiC power MOSFETs by soft gamma radiation and its correlation to the Terrestrial Cosmic Rays failure rate data as mesured by neutron irradiation," in *J021 IEEE International Reliability Physics Symposium (IRPS) | 978-1-7281-6893-7/21/$31.00 ©2021 IEEE | DOI: 10.1109/IRPS46558.2021.9405205*, 2021, vol. 53, no. 9, pp. 1689–1699.

[14] D. J. Lichtenwalner *et al.*, "Reliability studies of SiC vertical power MOSFETs," in *IEEE International Reliability Physics Symposium Proceedings*, 2018, vol. 2018-March, pp. 2B.21-2B.26, doi: 10.1109/IRPS.2018.8353544.

[15] M. Pocaterra and M. Ciappa, "TCAD investigation of the transport of carriers deposited by alpha particles in silicon carbide power Schottky devices," *Microelectron. Reliab.*, vol. 126, p. 114317, Nov. 2021, doi: 10.1016/j.microrel.2021.114317.

[16] M. Pocaterra and M. Ciappa, "Experimental setup to monitor non-destructive single events triggered by ionizing radiation in power devices," *Microelectron. Reliab.*, vol. 114, no. July, p. 113755, 2020, doi: 10.1016/j.microrel.2020.113755.

[17] Synopsys, "Sentaurus Device User," no. June, p. 2009, 2019.

[18] S. L. Miller, "Avalanche Breakdown in Germanium," *Phys. Rev.*, vol. 99, no. 4, pp. 1234–1241, Aug. 1955, doi: 10.1103/PhysRev.99.1234.

[19] T. Hatakeyama, "Measurements of impact ionization coefficients of electrons and holes in 4H-SiC and their application to device simulation," *Phys. Status Solidi Appl. Mater. Sci.*, vol. 206, no. 10, pp. 2284–2294, 2009, doi: 10.1002/pssa.200925213.

[20] L. Fursin and P. Losee, "Investigation of Terrestrial Neutron Induced Failure Rates in Silicon Carbide JFET Based Cascode FETs," vol. 2022 IEEE, pp. 8–13, 2022, doi: 10.1109/IRPS48227.2022.9764434.

[21] F. Principato, S. Altieri, L. Abbene, and F. Pintacuda, "Accelerated tests on Si and SiC power transistors with thermal, fastand ultra-fast neutrons," *Sensors (Switzerland)*, vol. 20, no. 11, pp. 1–15, 2020, doi: 10.3390/s20113021.